Static and high-frequency magnetic properties of nanocrystalline Fe-Zr-N films

Elena Sheftel[1], *Eugene* Harin[1], *Valentin* Tedzhetov[1,*], *Konstantin* Rozanov[2], *Polina* Zezyulina[2], *Stanislav* Bobrovskii[2], and *Philipp* Kiryukhantsev-Korneev[3]

[1]A.A. Baikov Institute of Metallurgy and Materials Science RAS, Moscow, Russia
[2]Institute for Theoretical and Applied Electromagnetics RAS, Moscow, Russia
[3]National University of Science and Technology "MISIS", Moscow, Russia

Abstract. The phase and structural states of nanocrystalline Fe-based films alloyed with Zr and N, which were prepared by reactive magnetron sputtering under different conditions, magnetic-structure parameters of the films and their static and high-frequency magnetic properties have been studied. The interrelation of static magnetic properties and magnetic-structure parameters with the value of real effective magnetic permeability μ' and frequency range, for which the value is unchanged, has been studied.

1 Introduction

The designing of miniature high-frequency induction electronic devices used for radiocommunication, data storage, etc., which operate in the high-frequency (up to gigahertz range) ac magnetic fields, is the today's trend of the modern microelectronics. Film amorphous and nanocrystalline soft magnetic materials intended for these devices should exhibit the high saturation magnetization M_s, high magnetic permeability μ under static conditions and in high-frequency ac magnetic fields, and high frequency of natural ferromagnetic resonance (nFMR) f_r, which should exceed operating frequencies of electronic device.

The ferromagnetic resonance effect in a film ferromagnet characterized by both high saturation magnetization M_s and effective magnetic anisotropy field H_{eff} can be shifted to the high-frequency (HF) range; in this case, the films should be characterized by high magnetic permeability $\mu = M_s/H_{eff}$ in the HF spectral range $f_r = \gamma(4\pi M_s H_{eff})^{1/2} = \gamma H_{eff} (4\pi\mu)^{1/2}$, where $\gamma = 2.9$ MHz/Oe [1-4]. Hence, one can see that these requirements for a material are conflicting, namely, to increase f_r, the H_{eff} should be increased; in this case, a decrease in $\mu = M_s/H_{eff}$ takes place.

It is known that H_{eff} is determined by the magnetic structure of a film ferromagnet [5, 6], which in its turn, is determined by preparation and heat-treatment conditions. Investigation of a correlation between the magnetic structure and both static and HF properties, in particular magnetic permeability μ, as well as the film ferromagnet preparation conditions pays the way to optimization of the magnetic anisotropy field H_{eff}.

Among soft-magnetic film materials studied in recent years, nanocrystalline Fe-Zr-N system films are of substantial interest for investigators. This is related, on the one hand, to the possibility to prepare such films in amorphous and nanocrystalline states, in particular, by magnetron sputtering, and, on the other hand, to the prospect to prepare such films with unique static and HF soft-magnetic properties [7-11].

The aim of the present work is to study the correlation between static magnetic properties, magnetic-structure parameters and a value of real effective magnetic permeability μ' in frequency range, in which μ' is unchanged (nFMR), of Fe-Zr-N films prepared by magnetron sputtering under different conditions.

2 Experimental

The Fe-Zr-N films were prepared by magnetron sputtering of the Fe-2.4 wt. % Zr target being a Fe disc with evenly distributed Zr chips. In the magnetron chamber under exposure to plasma flame there occurred surface melting of Fe and Zr forming different alloys of Fe-Zr system in the erosion zone. Before each sputtering, the target was heated above Curie temperature using plasma at which sputtering process was held. Deposition took place in gas atmosphere of Ar + 5 [%] N_2 or Ar + 15 [%] N_2 under total pressure of p_{Ar+N2} 0.3 Pa. As substrates, we used glass plates with the thickness of $d_s = 0.4$ mm. The thickness of prepared films was estimated by glow-discharge optical emission spectroscopy [12], which was performed on a Horiba Jobin Yvon Profiler-2 instrument; the thickness was $d_f = 1.2\pm0.2$ μm.

The phase composition and fine structure (the coherent domain size corresponding to the grain size $2R_c$ and the microstrain ε at grain scale) were studied by X-ray diffraction (XRD) analysis using a Rigaku Ultima IV diffractometer equipped with a graphite monochromator, CuK_α radiation, Bragg-Brentano geometry, and original

* Corresponding author: velmurad@ya.ru

software for full-profile Rietveld analysis [13].

Magnetic hysteresis loops were measured in magnetic fields up to 16 kOe using a LakeShore 7407 vibrating-sample magnetometer. The error of measurement of saturation induction, which is related to the difference in the shape and dimensions of Ni standard sample (3 mm in diameter) and used samples, did not exceed ~10%. Magnetic structure parameters were estimated by correlation magnetometry [6].

The microwave permeability of the films is measured by the stripline technique [14] using square-shaped plate samples 23 mm in the plate dimension. The technique involves calibration measurements of two samples with a known permeability to eliminate the measurement uncertainty appeared because of intrinsic non-uniformities in the measuring setup. The measurements are made in the frequency range of 0.1 to 2 GHz in two perpendicular directions (x and y). From the measured effective permeability of the sample, $\mu_{measured}$, the intrinsic permeability of the film, $\mu_{intrinsic}$, is found by equation $\mu_{measured} = 1 + p(\mu_{intrinsic} - 1)$, where $p = d_f/d_s \approx 0.003$ is the content of the ferromagnetic constituent in the sample.

3 Results and discussion

3.1 Phase composition and structure

According to XRD data, the films under study are either amorphous (in terms of X-ray diffraction) or nanocrystalline (Fig. 1), depending on the nitrogen content in the magnetron chamber. At the nitrogen content of 5%, the phase composition of prepared film consists of two nitride nanocrystalline phases, such as Fe_4N and Fe_3N with a grain size of 3-6 nm. As the nitrogen content in the magnetron chamber increases from 5 to 15%, the amorphous structure enriched in Fe is formed in the films (Table 1, Fig. 1a). According to our previous magnetic studies [15], the Fe-Zr-N films with the amorphous structure, which gives a wide reflection in X-ray diffraction patterns, consist of α-Fe-based ferromagnetic grains less than 2 nm in size.

Table 1. Phase composition and fine structure of studied films.

N_2 during deposition	Phase composition, vol. %	Lattice parameter, Å	Grain size $2R_c$, nm	Microstrain ε, %
15%	XRD amorphous	–	–	–
5%	Fe_4N 12.0±0.4	3.797±0.004	5.5±0.8	0.3±0.8
	Fe_3N 88.0±0.4	4.711±0.005 4.291±0.005	3.1±0.1	0.3±0.2

3.2 Static magnetic properties and magnetic structure

As is known, the origin of static coercivity and magnetic permeability in nanocrystalline ferromagnets is explained by a random magnetic anisotropy model [5,6]. According the model the local effective magnetic anisotropy at the grain scale ($D^{1/2}H_a$) is suppressed when the grain size $2R_c$ is less than the exchange interaction length R_L. In this case, uniform magnetization domains $2R_L$ (the stochastic domains) determined by exchange interaction are formed in the nanocrystalline ferromagnet and its magnetic hysteresis in low magnetic fields is determined by the magnetic anisotropy field at the stochastic domain scale ($D^{1/2}\langle H_a\rangle$). Note, that several the stochastic domain with different $D^{1/2}\langle H_a\rangle$ magnitude can be formed in the nanocrystalline ferromagnet. Here, we report results of determination of $D^{1/2}H_a$ and $D^{1/2}\langle H_a\rangle$ magnitudes and static magnetic properties of studied films.

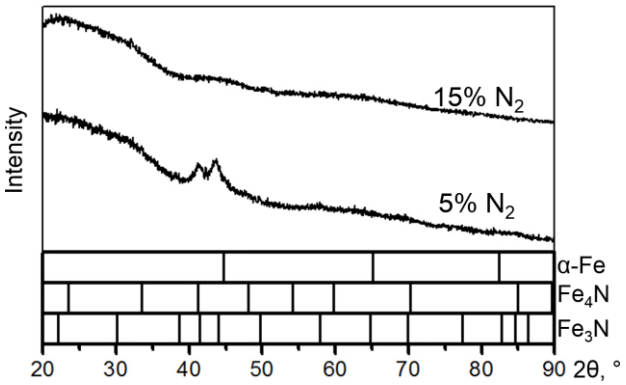

Fig. 1. XRD patterns of studied films deposited at the nitrogen content in the magnetron chamber of 15 and 5% N_2.

The shapes of hysteresis loops (Fig. 2) allow us to find the simultaneous presence of, at least, two main magnetic anisotropies differing in the value and symmetry. This is indicated by the change in the magnetization curve slope inwards the hysteresis loop in the first and third quadrants (Figs. 2a and 2b) and extended hysteresis-free portion of magnetization curve, which corresponds to the magnetization of more than half of film volume (Fig. 2a).

Magnetization curves in high magnetic fields are described by law of approach to magnetic saturation in terms of correlation magnetometry method [16]

$$M(H) = M_s[1 - (1/2)(D^{1/2}H_a)^2 / (H^2 + H^{1/2} H_R^{3/2})]. \quad (1)$$

Using Eq. (1) for the films under study, the saturation magnetization (M_s), the root-mean-square fluctuation of effective local (at the grain scale $2R_c$) anisotropy field ($D^{1/2}H_a$) and exchange field (H_R) were determined (Table 2). These magnitudes were used to estimate the first (of two anisotropy fields found from the hysteresis loop shape) anisotropy field of stochastic domain (Table 2): $D^{1/2}\langle H_a\rangle_1 = (D^{1/2}H_a)^4/H_R^3$.

Magnetization dispersion curves $1–M(H)/M_s$ plotted on log-log coordinates (insets on Fig. 3) indicate three asymptotes: (*I*) $1 - M(H) / M_s = (1 / 2) (D^{1/2}\langle H_a\rangle_2 / H)^2$, (*II*) $1 - M(H) / M_s = (1 / 2) (D^{1/2}H_a)^2 / (H^{1/2}H_R^{3/2})$ and (*III*) $1 - M(H) / M_s = (1 / 2) (D^{1/2}H_a / H)^2$. The curve connected the second and third asymptotes (*IV*) is described by Eq. (1). The second root-mean-square fluctuation of effective anisotropy field of stochastic domain $D^{1/2}\langle H_a\rangle_2$ (Table 2) was estimated using asymptote I.

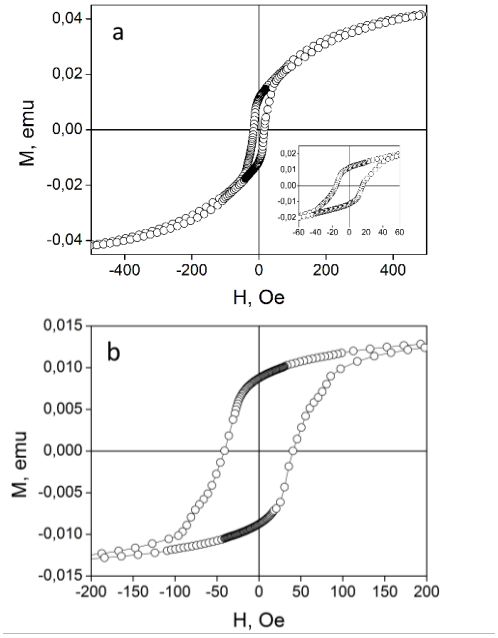

Fig. 2. The hysteresis loops of the studied films prepared with (a) 15 and (b) 5% N_2 in the magnetron chamber atmosphere.

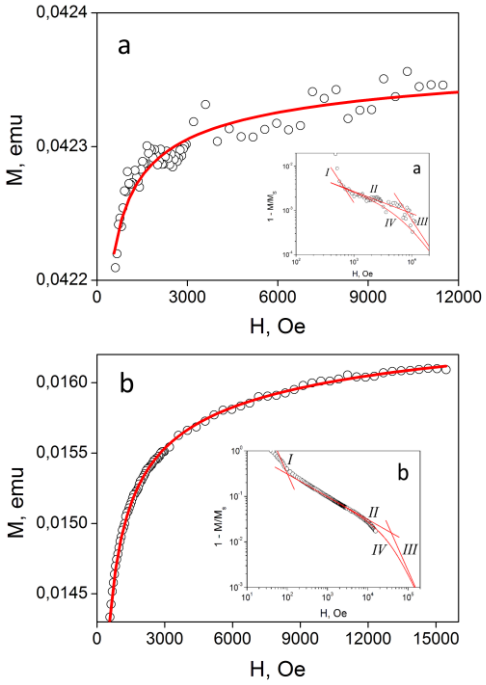

Fig. 3. High-field magnetization curves for the studied films prepared at a nitrogen content of (a) 15 and (b) 5% in the magnetron-chamber atmosphere. Solid lines are fitting by Eq. (1). Insets: magnetization dispersion curves ($1–M/M_s$) for the studied films prepared at a nitrogen content of (a) 15 and (b) 5% in the magnetron-chamber atmosphere. Solid lines are described in the text.

This means that the magnetic hysteresis in the studied films is induced by rotation of stochastic domains with different anisotropy filed magnitudes ($D^{1/2}\langle H_a\rangle_1$ and $D^{1/2}\langle H_a\rangle_2$, Table 2). In this case, in accordance with theoretical estimations [6], the coercive field of the film should be equal (to a certain approximation) to the anisotropy field of stochastic domains abundantly present in the magnetic structure.

Table 2. Parameters of magnetic structure of studied films.

N_2 content during depo-sition	M_s, G (T)	H_c, Oe	$D^{1/2}\langle H_a\rangle_1$, Oe	$D^{1/2}\langle H_a\rangle_2$, Oe	$D^{1/2}H_a$, Oe	H_R, Oe
15%	1060 ±270 1.3 ±0.3	16 ±1	0.03 ±0.01	90 ±70	350 ±150	8000 ±4500
5%	360 ±30 0.46 ±0.04	41 ±3	39 ±14	80 ±10	6900 ±400	38600 ±2700

3.3 High-frequency magnetic properties

The microwave permeability of the sample deposited in the atmosphere containing 5% N_2 is negligible as compared to the measurement error and is not discussed below. The measured microwave permeability of the sample produced at 15% nitrogen content is shown in Fig. 4 for two mutually perpendicular orientation of the film. The magnetic properties of the film are slightly anisotropic in the film plane. The magnetic loss peak observed at frequencies of about 700 MHz is due to the nFMR arising at the effective anisotropy field H_{eff} [8]. For thin films, the relation between nFMR frequency f_r and the effective anisotropy field is given by Kittel's equation,

$$f_r = \gamma(4\pi M_s H_{eff})^{1/2} \qquad (2)$$

where γ is gyromagnetic ratio. The values of H_{eff} estimated by Eq. (2) from the measured location of the magnetic loss peak are given in Table 3.

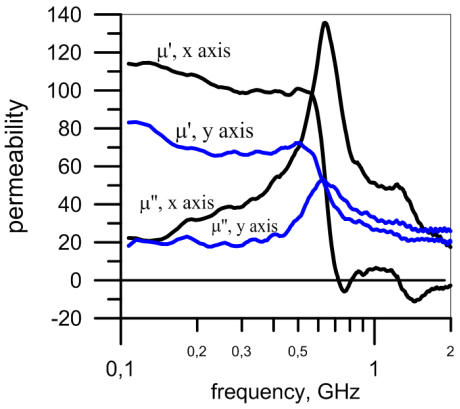

Fig. 4. The real (μ') and imaginary (μ'') permeability of the films, obtained in atmosphere with 15% N_2, measured along two mutually perpendicular directions, x and y.

It is seen from Tables 2 and 3 that, as the deposition conditions changes (5 and 15 %N_2 in magnetron-chamber atmosphere), the H_{eff} and H_c magnitudes demonstrate the similar character of variations. This agrees with data of [17], which showed that the H_{eff} magnitude should be proportional to the H_c coercive force magnitude. This indicates the fact that the static magnetic structure affects the dynamic magnetic properties. It should be noted that the measured

magnitudes (Table 3) depend on the measurement direction (*x* and *y*) and the fact that the unsmoothed magnetization permeability curves (Fig. 4) are likely to indicate the magnetic-structure inhomogeneity.

Table 3. HF magnetic permeability of the studied films.

N_2 content during deposition	Measure-ment direction	f_r, GHz	H_{eff}, Oe	μ'	f, GHz
15%*	*x*	0.7	4.3±0.8	80	0.58
	y	1.17	12.2±4	60	0.6
15%*	*x*	0.57	2.9±0.6	160	0.1
	y	0.64	3.7±0.8	130	0.1
5%	*x*	0.82	17.4±1.4	12	0.45
	y	0.72	13.5±1.1	12	0.3

* Two samples were deposited simultaneously.

The difference between field magnitudes H_{eff}, H_c and $D^{1/2}\langle H_a\rangle$ can be explained by decreasing scales at which they are realized, i.e., from macroscopic scale, H_{eff} for whole film, to the maximum fraction with a some magnetic anisotropy close to the H_c and, finally, to microscopic scale, for stochastic domain $D^{1/2}\langle H_a\rangle$. At a frequency of 1 GHz (the wavelength is 30 cm), the magnetic moment of whole film 2.3 cm in length is in resonance oscillations; this determines the H_{eff} magnitude. As it was noted above, the analysis of hysteresis loop shape allows us to assume the presence of, at least, two volumes differing in the magnetic anisotropy in the studied films, whereas the H_c field of the film is determined by the magnetic anisotropy of biggest volume. The $D^{1/2}\langle H_a\rangle$ field magnitude is determined from the high-field portion of magnetization curve (Fig. 3) and corresponds to the anisotropy field of stochastic micron-sized domain.

The real effective magnetic permeability μ' and the frequency range of its "operation" are the applied characteristics for high-frequency operation. Table 3 shows the μ' magnitudes for the studied films and the maximum f frequency for which the μ' value remains unchanged. Taking into account the measurement accuracy of the film thickness (1.2±0.2 μm), the error of measurement of μ' is ±17%. The measured μ' values qualitatively obey the relationship $\mu' = M_s/H_{eff}$. Note that the Fe-Zr-N films, in particular, $Fe_{89\text{-}88}Zr_{10}N_{11\text{-}12}$ [11,15], have the substantially higher M_s values as compared to those of the films studied in the present work, which reach 1.8-1.9 T. For the films with M_s =1.8-1.9 T, the higher f_r value and the higher permeability $\mu' = M_s/H_{eff}$ can be expected.

4 Conclusions

Nanocrystalline (with a grain size of 3-6 nm or < 2 nm) soft magnetic FeZrN films prepared by dc magnetron sputtering of the Fe – 2.4 wt% Zr target in the (Ar + N_2) atmosphere containing 5 and 15% N_2 have been studied. Parameters of magnetic structure ($D^{1/2}\langle H_a\rangle_1$, $D^{1/2}\langle H_a\rangle_2$, $D^{1/2}H_a$, H_R), saturation magnetization M_s (0.5-1.34 T), and magnetic permeability μ' (80-100) remained unchanged to frequencies of 500 GHz were determined. The dependence of the high-frequency magnetic permeability μ' and the ac magnetic-field frequency, at which the μ' magnitude remains unchanged, on the magnetic-structure parameters of the films was considered. It was shown that the static magnetic structure determines the dynamic magnetic properties.

This study was supported in part by the Russian Foundation for Basic Research (projects nos. 18-03-00502 and 18-08-00491).

References

1. S.X. Wang, N.X. Sun, M. Yamaguchi, S. Yabukami, Nature **407**, №6802, 150 (2000)
2. I. Kim, J. Kim, K.H. Kim, M. Yamaguchi, IEEE Trans. Magn. **40**, 2706 (2004)
3. S. Kong, T. Okamoto, Sh. Nakagawa, J. Appl. Phys. **93**, 6778 (2003)
4. I.T. Iakubov, A.N. Lagarkov, S.A. Maklakov, *et al.* J. Magn. Magn. Mat. **321**, 726 (2009)
5. G. Herzer, Acta Materialia **61**, 718 (2013)
6. R.S. Iskhakov, S.V. Komogortsev, Phys. of Metals and Metallography **112**, 666 (2011)
7. R.S. Iskhakov, M.M. Brushtunov, A.G. Narmonev, *et al.* Phys. Met. Metallogr. **79**, Iss. 5, 122 (1995)
8. C. Kittel, Phys. Rev. 73, 155 (1948)
9. O.M. Zhigalina, D.N. Khmelenin, A.L. Vasil'ev, E.N. Sheftel', *et al.* Cryst. Reports 58, 344 (2013)
10. E.N. Sheftel', E.V. Kharin, V.A. Tedzhetov, *et al.* Russian Metallurgy (Metally) **2016**, 826 (2016)
11. E.N. Sheftel, E.V. Harin, V.A. Tedzhetov, *et al.* Physica B **494**, 13 (2016)
12. Ph.V. Kiryukhantsev-Korneev, Protection of Metals and Physical Chemistry of Surfaces **48**, 585 (2012)
13. E.V. Shelekhov, T.A. Sviridova, Metal Science and Heat Treatment **42**, 309 (2000)
14. S.N. Starostenko, K.N.Rozanov, A.V. Osipov, J. Appl. Phys. **103**, 07E914 (2008)
15. E.N. Sheftel, V.A. Tedzhetov, E.V. Harin, *et al.* Phys. Stat. Sol. C **13**, 965 (2016)
16. S.V. Komogortsev, R.S. Iskhakov. J. Magn. Magn. Mat. **440**, 213 (2017)
17. S.S. Maklakov, S.A. Maklakov, I.A. Ryzhikov, *et al.* J. Magn. Magn. Mat. **324**, 2108 (2012)